View metadata, citation and similar papers at core.ac.uk
brought to you by CORE
provided by NASA Technical Reports Server

Improved prediction of quasi-global vegetation conditions using remotely-sensed surface soil moisture

Bolten J.D.[1], Crow W.T.[2]

[1]NASA Goddard Space Flight Center, Hydrological Sciences Lab, Greenbelt, MD 20771, USA, john.bolten@nasa.gov; [2]USDA Hydrology and Remote Sensing Lab, Bldg. 007, BARC-W, Beltsville, MD 20705, wade.crow@ars.usda.gov

The added value of satellite-based surface soil moisture retrievals for agricultural drought monitoring is assessed by calculating the lagged rank correlation between remotely-sensed vegetation indices (VI) and soil moisture estimates obtained both before and after the assimilation of surface soil moisture retrievals derived from the Advanced Microwave Scanning Radiometer-EOS (AMSR-E) into a soil water balance model. Higher soil moisture/VI lag correlations imply an enhanced ability to predict future vegetation conditions using estimates of current soil moisture. Results demonstrate that the assimilation of AMSR-E surface soil moisture retrievals substantially improve the performance of a global drought monitoring system - particularly in sparsely-instrumented areas of the world where high-quality rainfall observations are unavailable.

1. Introduction

Variations in soil moisture availability can provide a leading signal for subsequent anomalies in vegetative health and productivity [*Adegoke and Carleton,* 2002; *Ji and Peters,* 2003; *Musyim,* 2011]. As a result, soil moisture information is a key input into many large-scale drought monitoring systems [*Mo et al.*, 2010]. For example, the United States Department of Agriculture (USDA) Foreign Agricultural Service (FAS) attempts to anticipate the impact of drought on regional agricultural productivity by monitoring soil moisture conditions using a quasi-global soil water balance model [*Bolten et al.*,

2009]. However, the accuracy of such models is dependent on the quality of their required meteorological inputs and is thus questionable over data-poor regions of the globe.

With the onset of data availability from the ESA Soil Moisture and Ocean Salinity (SMOS) and NASA Soil Moisture Active and Passive (SMAP) L-band missions [*Kerr and Levine*, 2008; *Entekhabi et al.*, 2010], the next five years should see a significant expansion in our ability to retrieve surface soil moisture using satellite remote sensing. However, the added value of soil moisture remote sensing, above and beyond current water balance modelling approaches, has not yet been objectively quantified. Here, we evaluate the utility contributed by existing remotely-sensed surface soil moisture products for quasi-global agricultural drought monitoring. Following *Peled et al.* [2010] and *Crow et al.* [2012], our approach is based on sampling the lagged correlation between root-zone soil moisture anomalies obtained from a water balance model and subsequent anomalies in vegetation conditions (as captured by satellite-based visible/near-infrared vegetation indices). Since this approach measures the ability of current soil moisture estimates to anticipate future variations in vegetation health, it provides a direct valuation of soil moisture products in an agricultural drought context. In addition, by comparing correlations obtained before and after the assimilation of remotely-sensed surface soil moisture retrievals into the water balance model, we can quantify the added utility associated with assimilating remote sensing observations.

2. Methodology

2.1. 2-Layer Palmer Model

Model estimates of surface and root-zone soil moisture are derived from the 2-Layer Palmer water balance model currently used operationally by USDA FAS. The model is based on a bucket-type modeling approach as described in *Palmer* [1965]. The available water capacity (AWC) of the top model layer is assumed to be 2.54 cm at field capacity, and the AWC of the second layer (i.e., root-zone layer) is calculated using soil texture, depth to bedrock, and soil type derived from the Food and Agriculture Organization (FAO) Digital Soil Map of the World available from the FAO at http://www.fao.org/ag/agl/lwdms.stm#cd1. In this fashion, water holding capacity for both layers (incorporating near-surface soil moisture and groundwater) range between 2.54 cm to 30 cm according to soil texture and soil depth. Vertical coupling between the two model layers is calculated using a simple linear diffusion equation based on the soil moisture content of each layer and an assigned diffusion coefficient [*Bolten et al.*, 2010]. A confining layer (i.e., bedrock) is assumed for the bottom of the second model layer and is treated as a "no flow" boundary. Evapotranspiration is calculated from the modified FAO Penman-Monteith [*Allen et al.,* 1998] method and observations of daily min/max temperature. Further modeling details are available in *Bolten et al.* [2010]. Required daily rainfall accumulation and air temperature datasets are obtained from the U.S. Air Force Weather Agency (AFWA) Agriculture Meteorological (AGRMET) system (see http://www.mmm.ucar.edu/mm5/documents/DATA_FORMAT_HANDBOOK.pdf) which derives a daily rainfall accumulation product based on: microwave sensors on various polar-orbiting satellites, infrared sensors on geostationary satellites, a model-based cloud analysis, and World Meteorological Organization (WMO) surface gauge observations.

Despite its continued operational use, the 2-Layer Palmer model is obviously less complex than many more modern land surface models. However, using the same NDVI-based evaluation system applied here, *Crow et al.* [2013] found that modern land surface models generally offered only marginal increases in agricultural drought monitoring skill relative to simplistic soil water accounting models - suggesting that the 2-Layer Palmer model remains a reasonable baseline for evaluating the added impact of assimilating new remote sensing products.

All modeling is performed on a quasi-global (60° S to 60° N) domain and 0.25° resolution mesh using a daily time step between June 1, 2002 to December 31, 2010. Soil moisture conditions are initialized using climatologically-averaged values (2002 to 2010) for June 1, 2002 and spun-up until the start of the analysis on July 1, 2002. Soil moisture predictions obtained from the model alone will be referred to as open loop (OL) results.

2.2. Remotely-Sensed Soil Moisture

Surface soil moisture retrievals are obtained from gridded 0.25° Land Parameter Retrieval Model (LPRM) products provided by VU University Amsterdam based on Advanced Microwave Scanning Radiometer-EOS (AMSR-E) brightness temperature products [*Njoku et al,* 2003] between June 2002 and December 2010 [*de Jeu et al*., 2003; *Owe et al.,* 2008]. The effective measurement depth of LPRM surface soil moisture retrievals is estimated to be 1-2 cm. For the purposes of this analysis, we assume these retrievals reflect the equivalent soil moisture estimated in the surface layer of the 2-Layer Palmer model. Only descending (1:30 AM local time) overpasses are used since they appear to be more useful for soil moisture retrieval than ascending overpasses [*de Jeu*, 2003]. LPRM gridded products are screened to mask areas with frozen soil, snow cover,

and/or excessive vegetation using a surface temperature algorithm based on 37 GHz AMSR-E brightness temperature observations and retrieved canopy optical depth [*Owe et al.*, 2008].

2.3. The Ensemble Kalman Filter

Prior to assimilation, systematic biases between modeled and observed soil moisture datasets must be removed [*Kumar et al.*, 2012]. To eliminate these differences, raw LPRM surface soil moisture retreivals (θ_{LPRM}) are rescaled such that their inter-annual (2002 to 2010) mean (μ) and standard deviation (σ) obtained for a 31-day window centered on a given day-of-year (DOY) matches the mean and standard deviation sampled from the top-layer of an open-loop realization (OL1) of the model over the same time period:

$$\theta^{*}_{\mathrm{LPRM},i} = \left(\theta_{\mathrm{LPRM},i} - \mu_{\mathrm{LPRM}}^{\mathrm{DOY}(i)}\right)\frac{\sigma_{\mathrm{OL1}}^{\mathrm{DOY}(i)}}{\sigma_{\mathrm{LPRM}}^{\mathrm{DOY}(i)}} + \mu_{\mathrm{OL1}}^{\mathrm{DOY}(i)}. \qquad (1)$$

Note that all soil moisture variables in (1) and below are given in volumetric units [$m^3\ m^{-3}$].

The assimilation of θ^*_{LPRM} from (1) into the USDA FAS 2-Layer Palmer model is based on an Ensemble Kalman Filter (EnKF). A 30-member ensemble of two-element soil moisture state vectors $\boldsymbol{\theta}^j$ containing model surface and root-zone predictions is created via the direct perturbation of model soil-water balance calculations. These additive, mean-zero Gaussian perturbations are applied during each daily time step of the model and have covariance:

$$\mathbf{Q} = \begin{bmatrix} Q & \alpha Q \\ \alpha Q & \alpha^2 Q \end{bmatrix} \qquad [\mathrm{m}^6\ \mathrm{m}^{-6}], \qquad (2)$$

where α is the ratio of surface layer AWC to root-zone AWC. Upon acquisition of θ^*_{LPRM} at time i via the rescaling step in (1), each ensemble replicate $\boldsymbol{\theta}^j$ is updated following

$$\boldsymbol{\theta}_i^{j+} = \boldsymbol{\theta}_i^{j-} + \mathbf{K}_i\left[\theta^*_{\mathrm{LPRM},i} + \varepsilon_i^j - \mathbf{H}\boldsymbol{\theta}_i^{j-}\right], \quad (3)$$

where the observation operator $\mathbf{H}$ = [1 0]; ε is mean-zero, Gaussian noise with variance R [m^6 m^{-6}]; and j is an ensemble number index. The Kalman gain vector $\mathbf{K}$ in (3) is

$$\mathbf{K} = \mathbf{P}\mathbf{H}^T/(\mathbf{H}\mathbf{P}\mathbf{H}^T + R), \quad (4)$$

with $\mathbf{P}$ representing the 2 x 2 state covariance matrix sampled directly from the $\boldsymbol{\theta}_i^{j-}$ ensemble (created, in part, by the introduction of noise with covariance $\mathbf{Q}$) and R the scalar error variance of θ^*_{LPRM} retrievals. While θ^*_{LPRM} is assumed to directly reflect surface layer conditions, the covariance information in $\mathbf{P}$ is used to update both surface and root-zone forecasts contained in $\boldsymbol{\theta}_i^{j-}$. After updating, each $\boldsymbol{\theta}_i^{j+}$ replicate is propagated in time by the Palmer 2-Layer Model (and further perturbed via $\mathbf{Q}$) until the next-available θ^*_{LPRM} observation, at which point (3) is re-applied using a newly sampled $\mathbf{P}$. Daily EnKF state predictions for the surface and root-zone layers, θ_{EnKF1} and θ_{EnKF2} respectively, are then obtained by averaging across the resulting $\boldsymbol{\theta}_i^{j+}$ ensemble.

The parameter R represents the error variance in θ^*_{LPRM} retrievals for a given land surface type. The skill of retrieved soil moisture decreases significantly over areas of dense vegetation [*Njoku and Chan*, 2006]. Therefore, following *Bolten et al.* [2010], we calculate R as

$$R = R_0 \exp[2(\cos^{-1}(\varphi) b \omega_c)], \quad (5)$$

where φ is the AMSR-E incidence angle; b [m^2 kg^{-1}] is a vegetation structure coefficient (set equal to 0.30 for wooded grasslands and shrubs, grasslands, and croplands and 0.28 for closed bushlands, open shrublands, and bare soil); ω_c [kg m^{-2}] is canopy vegetation

water content; and R_o is a constant set equal to 0.15^2 cm^6cm^{-6}. A monthly climatology of Advanced Very High Resolution Radiometer-derived NDVI retrievals is used to estimate ω_c following *Bindlish et al.* [2003]. While (5) has already been applied successfully for use in a similar data assimilation system [*Bolten et al.*, 2010], it should be noted that more complex error estimates for θ_{LPRM} retrievals are also available [*Parinussa et al.*, 2011].

Likewise, Q captures the added uncertainty incurred when the 2-Layer Palmer advances soil moisture estimates ahead by a one day. Here we assume Q is driven primarily by the accuracy of daily rainfall accumulation products used to force the model. Since this accuracy is known to vary geographically according to the density of available rain gauges for the correction of satellite-based rainfall estimates [*Gebremichael et al*, 2003], Q is specified as a function of the average distance D [km] to the three-closest WMO rain gauges:

$$Q = \begin{cases} 0.02^2\ \mathrm{m^6 m^{-6}} & D < 100\ \mathrm{km} \\ 0.04^2\ \mathrm{m^6 m^{-6}} & 100\ \mathrm{km} \le D < 150\ \mathrm{km} \\ 0.06^2\ \mathrm{m^6 m^{-6}} & 150\ \mathrm{km} \le D < 200\ \mathrm{km} \end{cases}. \quad (6)$$

For the case D >= 200 km: $Q = 0.08^2$ cm^6cm^{-6} and $R = 0$.

2.4. MODIS NDVI and Land Cover Data

Monthly Normalized Difference Vegetation Index (NDVI) products for evaluation are obtained from the Moderate Resolution Imaging Spectroradiometer (MODIS) MOD13C2 product [*NASA Land Processes DAAC*, 2011]. Monthly NDVI composite products categorized as “fully reliable” in the MOD13C2 reliability flag file are aggregated from their native 0.05° resolution to match the 0.25° resolution modeling grid. In order to focus on water-limited ecosystems, sub-grid fractions of barren, tundra,

forest cover, and open water surfaces from the MODIS MCD12C1 land cover classification [*NASA Land Processes DAAC*, 2010] are summed within each global 0.25° pixel, and pixels where the sum of these areas constitutes more than a 50% areal fraction are masked.

3. Analysis

3.1. Rank Correlation Sampling

Daily root-zone soil moisture estimates obtained from the 2-Layer Palmer model open loop (θ_{OL2}) and analysis products produced by the EnKF-based assimilation of θ^*_{LPRM} into the 2-Layer Palmer model (θ_{EnKF2}) are separately aggregated in time between July 2002 and December 2010 to obtain monthly $\overline{\theta_{\mathrm{OL2}}}$ and $\overline{\theta_{\mathrm{EnKF2}}}$ time series. Any months containing five or fewer θ_{LPRM} retrievals (e.g., due to snow cover and/or excessive vegetation) are masked from this monthly product. Each product is then grouped by month-of-year and ranked according to soil moisture value within these groupings. The resulting rank time series of Rank($\overline{\theta_{\mathrm{OL2}}}$) and Rank($\overline{\theta_{\mathrm{EnKF2}}}$) describe the wetness of any particular month relative to the same month in all other years of the 2002 to 2010 data record.

An analogous aggregation and ranking procedure is applied to monthly MODIS-based NDVI to obtain Rank($\overline{\mathrm{NDVI}}$), and the Spearman correlation coefficient $R_s(L)$ is sampled between Rank($\overline{\mathrm{NDVI}}$) for month k and both Rank($\overline{\theta_{\mathrm{OL2}}}$) and Rank($\overline{\theta_{\mathrm{EnKF2}}}$) for month $k+L$. Much of our analysis will focus on the specific case $R_s(-1)$ where L = -1, and rank correlation is calculated between monthly soil moisture and NDVI when soil moisture precedes NDVI by one month. Note that since neither the 2-Layer Palmer model nor LPRM utilizes NDVI information (and the EnKF uses only climatological NDVI

information which will not impact inter-annual ranks), sampled R_s should not be spuriously impacted by the presence of cross-correlated errors. To focus on periods of the annual cycle prone to water (and not energy) limitation, only months with an average daily high air temperature above 5° C are included in such sampling. A minimum threshold of at least 30 monthly $\overline{\mathrm{NDVI}}$ and $\overline{\theta_{\mathrm{OL2}}}$ (or $\overline{\theta_{\mathrm{EnKF2}}}$) pairs is then required to sample a reliable estimate of R_s.

3.2. Results

Figure 1 shows $R_s(L)$ on a global 0.25° degree grid for the model-only $\overline{\theta_{\mathrm{OL2}}}$ product [$R_s(\text{-}1)^{\mathrm{OL2}}$; Figure 1a] and the $\overline{\theta_{\mathrm{EnKF2}}}$ analysis [$R_s(\text{-}1)^{\mathrm{EnKF2}}$; Figure 1b]. Figure 1c plots the difference obtained by subtracting Figure 1b from Figure 1a (i.e., R_s^{EnKF2} minus R_s^{OL2}). By applying a Fisher transformation, *Z*-scores for this difference are calculated as

$$Z = \sqrt{\frac{n-3}{2*1.06}}\left[F(R_S^{\mathrm{EnKF2}}) - F(R_S^{\mathrm{OL2}})\right] \qquad (7)$$

where $F(R_s) = 0.5\ \mathrm{Ln}[(1+R_s)/(1-R_s)]$, n is the number of monthly soil moisture/NDVI values sampled to obtain R_s, and the factor 1.06 corrects for the non-Gaussian distribution of sampled R_s [*Fieller et al.*, 1957]. Resulting *Z*-scores are plotted in Figure 1d. Note that since (7) neglects both the presence of auto-correlation in Rank($\overline{\theta_{\mathrm{OL2}}}$) and Rank($\overline{\theta_{\mathrm{EnKF2}}}$) and potential cross-correlation in sampling error, care should be exercised in formally interpreting Figure 1d. Blank areas in Figure 1 are due to pixels failing the land-cover masking criteria described in Section 2.4 or land pixels where less than 30 pairs of values are available for estimating $R_s(\text{-}1)$ (see Section 3.1).

Arid regions (e.g., the Western United States, Southern Africa, and Australia) generally demonstrate the highest coupling between open loop root-zone soil moisture and future NDVI (Figure 1a). However, a sharp jump in $R_s(\text{-}1)$ is noted when θ^*_{LPRM} is

assimilated into the model (Figures 1b and 1c). The benefit of surface soil moisture data assimilation is especially large in areas of world where poor rain-gauge coverage degrades the quality of model-only $\overline{\theta_{\mathrm{OL2}}}$ estimates (e.g., Africa, Central Australia, and Central Asia). In these areas, the assimilation of θ^*_{LPRM} improves monthly-scale soil moisture estimates by filtering random modeling errors due to poorly-observed rainfall. In addition to the L = -1 case shown in Figure 1, qualitatively similar results (not shown) are also found for the cases L = -2 and -3 [months]. Finally, Figure 1d demonstrates that spatially continuous areas of enhanced $R_s(-1)$ are statistically significant at a 1σ level, and only sporadic areas of significantly degraded $R_s(-1)$ are found.

As seen in Figure 1, the impact of θ^*_{LPRM} assimilation is especially large in data-poor areas of world lacking sufficient ground-based rain gauge instrumentation for adequate correction of satellite-based rainfall products. A number of these notably data-poor countries also face considerable food security challenges. Figure 2 shows $R_s(L)^{\mathrm{OL2}}$ and $R_s(L)^{\mathrm{EnKF2}}$ results averaged within six countries in Africa and Southern Asia with moderate to severe food security issues. Relative to the model-only case, the EnKF data assimilation case demonstrates consistently stronger rank correlation with future NDVI in these countries.

It is also useful to examine seasonal trends in $R_s(-1)$. For both the Extra-Tropical Northern Hemisphere (ETNH; to 60° N) and Southern Hemisphere (ETSH; to 60° S), spatially-averaged $R_s(-1)^{\mathrm{OL2}}$ and $R_s(-1)^{\mathrm{EnKF2}}$ are plotted in Figure 3 as a function of month-of-year. The seasonal time series in Figure 3 demonstrates an intuitive pattern with the highest soil moisture/NDVI coupling, and thus the largest $R_s(-1)$, occurring during the middle/end of ETNH and ETSH summers when soil moisture storage tends to

be at yearly low. An increase in spatially-averaged $R_s(-1)^{EnKF2}$ (relative to $R_s(-1)^{OL2}$) is apparent throughout the annual cycle. In particular, despite relatively high levels of biomass, and thus reduced accuracy in remotely-sensed surface soil moisture retrievals [*Njoku and Chen*, 2006] during the ETNH and ETSH summers, the positive impact of soil moisture data assimilation persists throughout the growing season. This ability to add skill in the middle portion of the growing season is critical since crop yield sensitivity to water stress is maximized during this period.

4. Conclusions

Agricultural drought is commonly defined as an extended period of lower than normal root-zone soil moisture characterized by a reduction in plant biomass and ecologic productivity. Here, we quantify the added value of remotely-sensed surface soil moisture retrievals for improving our ability to accurately predict agricultural drought impacts on regional vegetation productivity. Following the general approach of *Peled et al.* [2010], our evaluation is based on sampling the rank correlation between current monthly root-zone soil moisture and future NDVI conditions.

The assimilation of surface soil moisture retrievals into a quasi-global soil water balance model is shown to significantly improve the value of model-based, root-zone soil moisture estimates as a leading indicator of agricultural drought (Figure 1). Such improvement is especially clear over data-poor regions of the world where modeled soil moisture estimates are derived from poor-quality rainfall observations (Figure 2). Value is added even during the middle portion of the growing season when both vegetation biomass and crop yield sensitivity to drought is maximized (Figure 3). Overall, results provide an important new verification of the potential of remotely-sensed surface soil

moisture for regional-scale agricultural and ecological prediction activities - particularly in water-limited and/or data-poor regions of the world prone to food insecurity. While the use of vegetation indices like NDVI as a proxy variable for yield is well-established [*Becker-Reshef et al.*, 2010], a better characterization of agricultural productivity can be obtained from comparison against actual crop yield data. In addition, to fully characterize their utility for rapid drought and famine response, soil moisture estimates should ideally be evaluated at finer temporal scales (e.g., weekly rather than monthly). Finally, at least two more years of additional SMOS data collection is required to apply a comparable analysis to L-band satellite soil moisture products. Consequently, results in this paper should be interpreted only as a feasibility analysis and not as the description of a finalized agricultural drought product.

Acknowledgements

Research was funded by a grant from the NASA Applied Sciences Program.

References

Adegoke, J. O., and A.M. Carleton (2002), Relations between soil moisture and satellite vegetation indices in the U.S. Corn Belt, *J. Hydrometeorol.*, *3*(4), 395-405.

Allen, R. G., L. S. Pereira, D. Raes, M. Smith (1998), Crop evapotranspiration - guidelines for computing crop water requirements- Food and Agriculture Organization - Irrigation and Drainage Paper 56, 27-65.

Becker-Reshef, I., C. O. Justice, M. Sullivan, E. Vermote, C. Tucker, A. Anyamba, J. Small, E. Pak, E. Masouka, J. Schmaltz, M. Hansen, K. Pittman, C. Birkett, D. Williams, C. Reynolds, B. Doorn (2010), Monitoring global croplands with coarse resolution earth observations: The Global Agriculture Monitoring (GLAM) project, *Remote Sens*., *2*(6), 1589-1609.

Bindlish R., T. J. Jackson, E. Wood, H. Gao, P. Starks, D. Bosch (2003), Soil moisture estimates from TRMM microwave imager observations over the southern United States, *Rem. Sens. Environ.*, *85*(4), 507 - 515.

Bolten, J. D., W. T. Crow, T. J. Jackson, X. Zhan and C. A. Reynolds (2010), Evaluating the utility of remotely-sensed soil moisture retrievals for operational agricultural drought monitoring, *IEEE J. Sel. Topics Appl. Earth Observ., 3*(1), 57-66.

Bolten, J. D., W. T. Crow, X. Zhan, C. Reynolds, T. J. Jackson, Assimilation of a satellite-based soil moisture product in a two-layer water balance model for a global crop production decision support system (2009), in *Data Assimilation for Atmospheric, Oceanic, and Hydrologic Applications*, Springer-Verlag.

Crow, W. T., S. V. Kumar, and J. D. Bolten (2012), On the utility of land surface models for agricultural drought monitoring, *Hydrol. Earth Syst. Sci.,, in press*.

de Jeu, R. (2003) Retrieval of Land Surface Parameters using Passive Microwave Remote Sensing, Ph.D. Dissertation, 120 pp., Vrije University Amsterdam, Amsterdam, the Netherlands.

Entekhabi, D., E. Njoku, P. O'Neill, K. Kellogg, W. Crow, W. Edelstein, J. Entin, S. Goodman, T. Jackson, J. Johnson, J. Kimball, J. Piepmeier, R. Koster, N. Martin, K. McDonald, M. Moghaddam, S. Moran, R. Reichle, J. Shi, M. Spencer, S. Thurman, L. Tsang, and J. Van Zyl (2010), The Soil Moisture Active and Passive (SMAP) Mission, *IEEE Proceed*., *98*(5), 704-716.

Fieller, E. C., H. O. Hartley, and E. S. Pearson (1957), Tests for rank correlation coefficients, *Biometrika*, *44*(3/4), 470–481.

Gebremichael, M., W. Krafewski, M. Morrissey, D. Langerud, G. Huffman, R. Adler (2003), "Error uncertainty analysis of GPCP monthly rainfall products: A data-based simulation study, *J. Appl. Met.*, *42(*12*)*, 1837-1848.

Jackson, T. J. and T. J. Schmugge (1991), Vegetation effects on the microwave emission of soils," *Rem. Sen. Environ.*, *36*(3), 203-212.

Ji, J. and A. J. Peters (2003), Assessing vegetation response to drought in the northern Great Plains using vegetation and drought indices, *Remote Sens. Environ.*, *87*(1), 85−98.

Kerr, Y. H. and D. Levine (2008), Forward to the special issue on the Soil Moisture and Ocean Salinity (SMOS) mission, *IEEE Trans. Geosci. Rem. Sens.*, *46*(3), 583–585.

Kumar, S., R. H. Reichle, K. W. Harrison, C. D. Peters-Lidard, S. Yatheendradas, and J. A. Santanello (2012), A comparison of methods for a priori bias correction in soil

moisture data assimilation, *Water Resour. Res. 48* W03515, doi:10.1029/2010WR010261.

Mo, K. C., L. N. Long, Y. Xia, S. K. Yang, J. E. Schemm, and M. B. Ek (2010), Drought indices based on the Climate Forecast System Reanalysis and ensemble NLDAS, *J. Hydrometeorol*., *12*(2),185-210.

Musyim, Z (2011), Temporal Relationships Between Remotely-Sensed Soil Moisture and NDVI over Africa: Potential for Drought Early Warning, M.S. Thesis, Dept. of Geo-Inform. Science and Tech., U. of Twenty, Enschede, The Netherlands.

NASA Land Processes Distributed Active Archive Center (2010), MODIS MCD12C1 (Collection 5). USGS/Earth Resources Observations and Science (EROS), Sioux Falls, South Dakota.

NASA Land Processes Distributed Active Archive Center (2011), MODIS MYD13C2 (Collection 5). USGS/Earth Resources Observations and Science (EROS), Sioux Falls, South Dakota.

Njoku, E. G. and S. K. Chan (2006), Vegetation and surface roughness effects on AMSR-E land observations," *Rem. Sens. Environ.*, *100*(2), 190–199.

Njoku, E. G., T. J. Jackson, V. Lakshmi, T. K. Chan, S. V. Nghiem (2003), Soil moisture retrieval from AMSR-E, *IEEE Trans. Geosci. Rem. Sens.*, *41*(2), 215-229.

Owe, M., R. De Jeu, and T. Holmes (2008), Multi-sensor historical climatology of satellite-derived global land surface moisture, *J. Geophys. Res.*, *113*, F01002, doi:1029/2007JF000769.

Palmer, W.C. (1965), Meteorological Drought, *U.S.* Weather Bureau Res. Paper 45.

Parinussa, R., A. G. C. A. Meesters, Y. Liu, W. Dorigo, W. Wagner, and R. A. M. De Jeu (2011), An analytical solution to estimate the error structure of a global soil moisture dataset, *IEEE Trans. Geosci. Rem. Sens.*, 8, 779-783, doi: 10.1109/LGRS.2011.2114872.

Peled, E., E. Dutra, P. Viterbo, and A. Angert (2010), Technical Note: Comparing and ranking soil drought indices performance over Europe, through remote sensing of vegetation, *Hydrol. Earth Syst. Sci., 14*, 271-277.

Figure 1. Global analysis of $R_s(-1)$ (i.e. the rank correlation between monthly soil moisture and NDVI when soil moisture precedes NDVI by one month) for: a) model-only (root-zone) soil moisture [$R_s(-1)^{OL2}$] and b) EnKF (root-zone) soil moisture created by assimilating LPRM soil moisture into the model [$R_s(-1)^{EnKF2}$]. Also plotted are c) $R_s(-1)^{EnKF2}$ minus $R_s(-1)^{OL2}$ (reflecting the net impact of the assimilating LPRM retrievals) and d) *Z*-scores for $R_s(-1)^{EnKF2}$ minus $R_s(-1)^{OL2}$ given by (7).

Figure 2. Comparisons between $R_s(\mathrm{L})^{OL2}$ and $R_s(\mathrm{L})^{EnKF2}$ over a range of L (i.e., 0 to 6 months) for sparsely-instrumented countries with moderate-to-severe food security issues. Plotted variable $R_s(L)$ is the rank correlation between monthly soil moisture for month $i+L$ and NDVI for month i.

Figure 3. Seasonal cycles of $R_s(-1)^{OL2}$ and $R_s(-1)^{EnKF2}$ averaged within the Extra-tropical Northern (ETNH; to 60° N) and Southern (ETSH; to 60° S) Hemispheres. Plotted variable $R_s(-1)$ is the rank correlation between monthly soil moisture and NDVI when soil moisture precedes NDVI by 1 month.

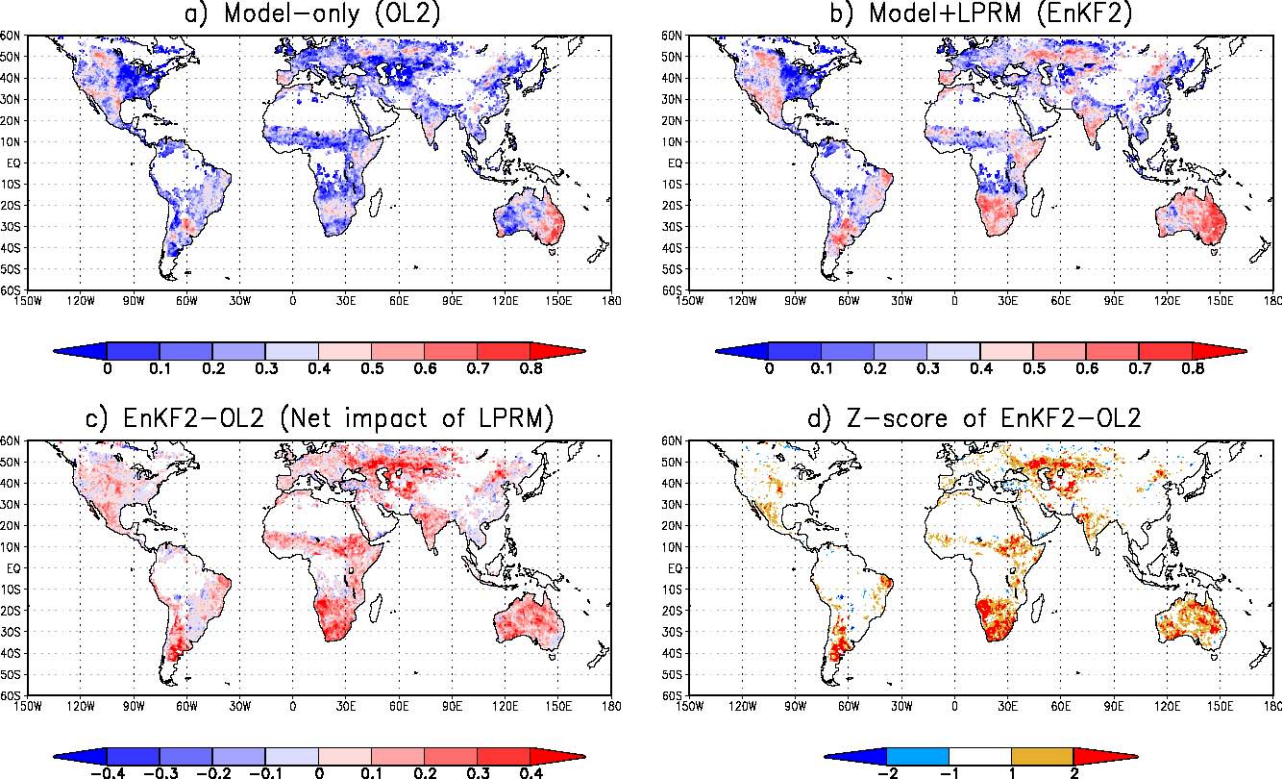
a) Model−only (OL2)
b) Model+LPRM (EnKF2)
c) EnKF2−OL2 (Net impact of LPRM)
d) Z−score of EnKF2−OL2
60N
50N
40N
30N
20N
10N
EQ
10S
20S
30S
40S
50S
60S
150W
120W
90W
60W
30W
0
30E
60E
90E
120E
150E
180
0 0.1 0.2 0.3 0.4 0.5 0.6 0.7 0.8
−0.4 −0.3 −0.2 −0.1 0 0.1 0.2 0.3 0.4
−2 −1 1 2

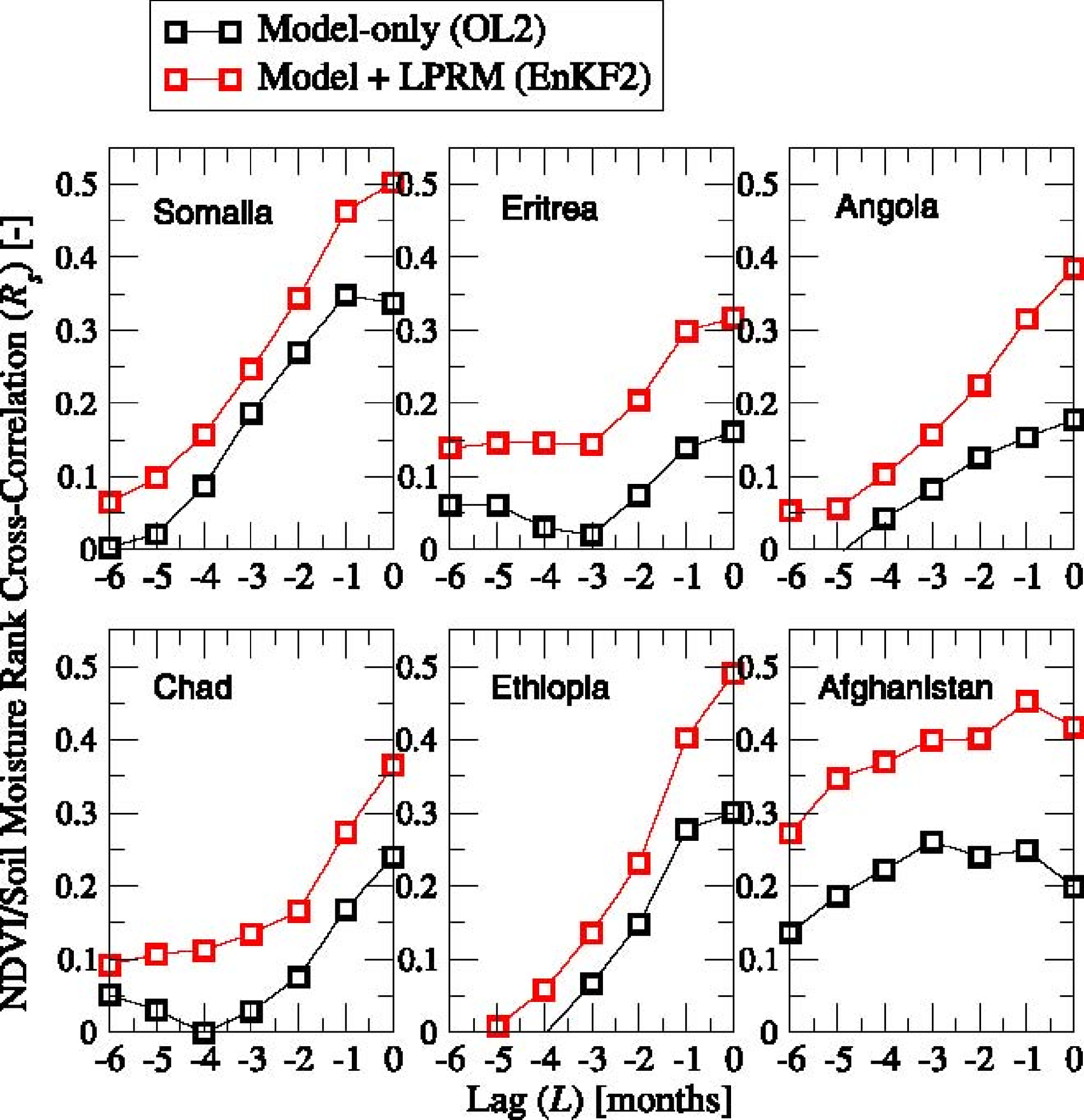
Model-only (OL2)
Model + LPRM (EnKF2)
Somalia
Eritrea
Angola
Chad
Ethiopia
Afghanistan
NDVI/Soil Moisture Rank Cross-Correlation (R_ρ) [-]
Lag (L) [months]
0
0.1
0.2
0.3
0.4
0.5
-6
-5
-4
-3
-2
-1
0

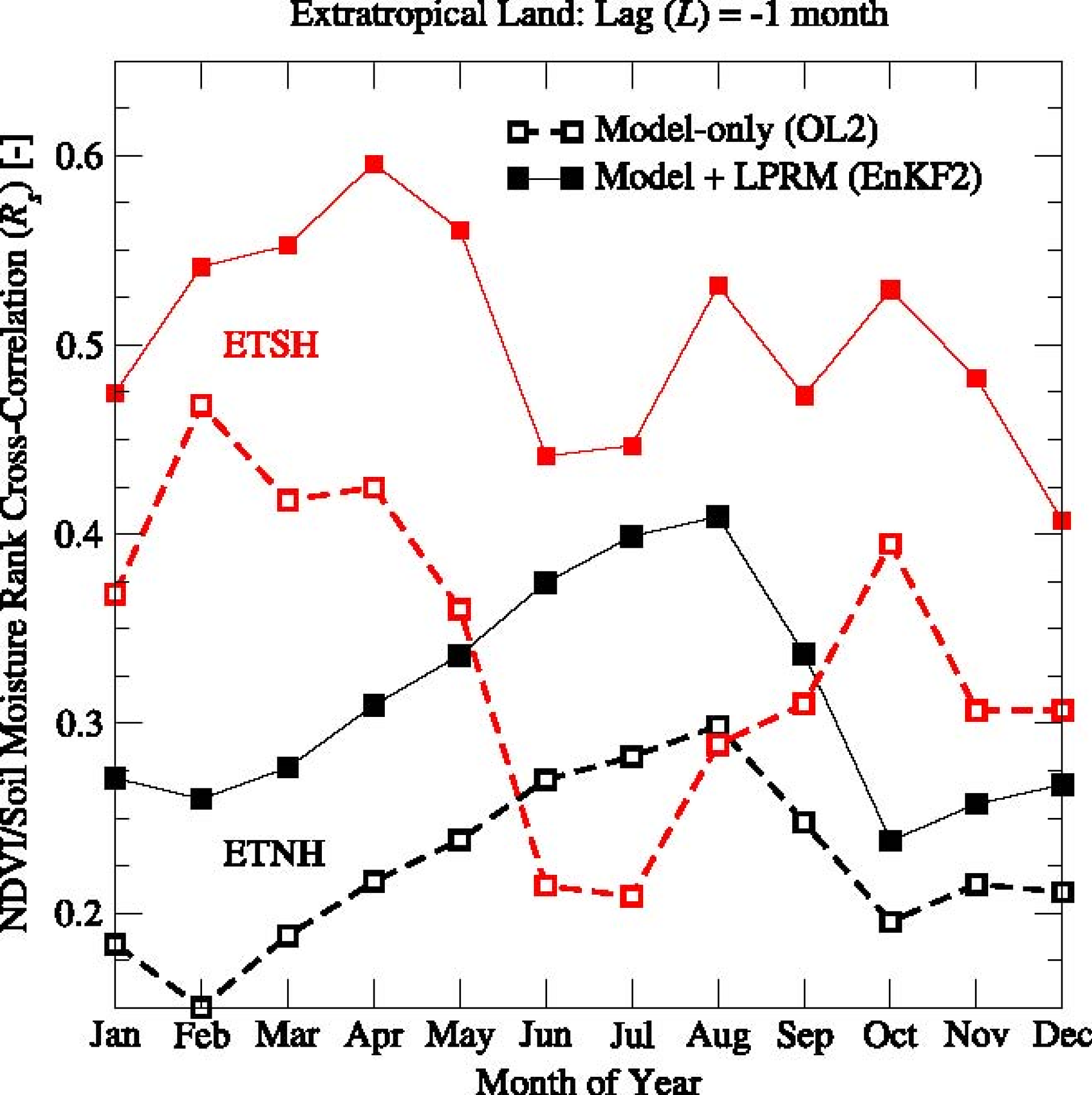
Extratropical Land: Lag (L) = -1 month
Model-only (OL2)
Model + LPRM (EnKF2)
ETSH
ETNH
NDVI/Soil Moisture Rank Cross-Correlation (R_s) [-]
0.2
0.3
0.4
0.5
0.6
Jan
Feb
Mar
Apr
May
Jun
Jul
Aug
Sep
Oct
Nov
Dec
Month of Year